having here angles of ±45° with the crystallographic *b* and *c* axes. The C_2 (pseudo-S_4) axes of the two magnetically inequivalent Mn(V) polyhedra are now perpendicular with respect to one another. While the MnO_4^{3-} polyhedra adapt the geometry and orientation of the host tetrahedra in the vanadate and arsenate without significant changes, this is apparently not so for the phosphate. Not only is the extent of the compression much larger than the one that characterizes the PO_4^{3-} tetrahedra in $Ca_2(PO_4)Cl$ (Tables II and IV), but also the orientation of the MnO_4^{3-} tetrahedra seems to be different (by ≈10°) from those of the PO_4^{3-} entities, which may be explained by packing forces due to the considerably larger ionic radius of Mn(V) compared to P(V).

Single-crystal EPR measurements were also performed with various apatite-type compounds. We were not able to analyze the angular dependencies of the **D** tensor, however. Presumably D_z, D_y, and D_x do not follow the approximate C_{3v} symmetry of the three magnetically inequivalent MO_4^{3-} polyhedra in the unit cell.

Conclusions and Summary

Strong d–d bands for both Mn(V) and Mn(VI) in tetrahedral oxo coordination are found around 16 000 cm^{-1} (Figure 2). Though the two spectra are quite different in their special features, a charge-transfer band is present at about 24 000 cm^{-1} for Mn(VI), while there is no significant absorption at these wavenumbers for Mn(V). At higher Mn(V) concentrations charge-transfer bands may move into the visible region also in this case. Both cations may induce green and blue colors. The color-determining minimum can be shifted from ≈20 000 cm^{-1} (green) to ≈22 000 cm^{-1} (blue) by geometric packing effects (compression due to small host site cations), by symmetry reduction (splittings and broadening of bands in the visible region), and by varying the concentration of manganese in the host compound.

Mn(V) and Mn(VI) can easily be distinguished by their EPR spectra in crystalline compounds with low doping concentrations, because well-resolved triplet transitions are observed for the d^2 configuration. At higher manganese concentrations, however, the triplet spectrum collapses to one signal at $g \approx 1.96$ as the consequence of exchange interactions. Because the half-field signal (H_{min}) is very weak in these cases and Mn(VI) induces an EPR signal also at $g \approx 1.96$, a discrimination between the two oxidation states may be difficult.

The EPR triplet spectra of Mn(V) together with the ligand spectra have been shown to be very informative with respect to the electronic ground state and the geometry and the volume of the MnO_4^{3-} polyhedron in the respective host compound. It was possible to derive from the single-crystal EPR spectra of various spodiosite-type compounds the specific differences in the geometry and the polyhedron orientation of the MnO_4^{3-} entities in comparison to the host tetrahedra. Thus, in the $Ca_2(PO_4)Cl$ host structure the S_4 directions of the two magnetically inequivalent MnO_4^{3-} polyhedra are oriented perpendicular to each other, compared to the angle of 72° between the PO_4^{3-} host polyhedra. Besides this misorientation of about 10°, the MnO_4^{3-} polyhedra exhibit a comparatively much stronger flattening than the PO_4^{3-} entities. Both effects are due to the considerably larger ionic radius of Mn(V) with respect to P(V) (Table I)[4] and presumably induced by packing forces in the unit cell.

Acknowledgment. Financial support by the Deutsche Forschungsgemeinschaft and the Fonds der chemischen Industrie is gratefully acknowledged.

Registry No. $Ca_2(PO_4)Cl$, 12013-61-5; $Ca_2(VO_4)Cl$, 12350-23-1; $Ca_2(AsO_4)Cl$, 12523-00-1; $Sr_2(VO_4)Cl$, 12410-18-3; Li_3VO_4, 15593-56-3; Li_3AsO_4, 13478-14-3; Li_3PO_4, 10377-52-3; $Ba_5(PO_4)_3Cl$, 12356-32-0; $Sr_5(PO_4)_3Cl$, 11088-40-7; Mn, 7439-96-5.

Contribution from the Institut für Physikalische und Theoretische Chemie, Universität Regensburg, D-8400 Regensburg, Federal Republic of Germany, and Institute of Inorganic Chemistry, University of Fribourg, CH-1700 Fribourg, Switzerland

Spectroscopic Studies of Cyclometalated Platinum(II) Complexes: Optical Absorption and Emission of Single-Crystal *cis*-Bis(benzo[*h*]quinolinato)platinum(II)

R. Schwarz,[†] G. Gliemann,*[,†] Ph. Jolliet,[‡] and A. von Zelewsky*[,‡]

Received August 30, 1988

The influence of temperature (1.9 K ≤ *T* ≤ 60 K) and high magnetic fields (0 ≤ *H* ≤ 6 T) on the optical properties of single-crystal *cis*-bis(benzo[*h*]quinolinato)platinum(II) (=[Pt(bhq)$_2$]) is reported. The analysis of the polarized optical absorption and emission spectra and of the excitation spectra indicates the existence of distinct X-traps, each being provided with two electronic excited states situated energetically below the lowest exciton band. At *T* = 1.9 K a luminescence of sharp-lined structure has been observed that is a superposition of the emissions from the respective lowest excited states of the traps. Increasing temperature depopulates these states and repopulates intermediately the trap states of higher energy and finally the exciton bands, resulting in an additional fine structure and a fictitious blue shift of the emission, respectively. When a magnetic field **H**∥*b* (**H** = magnetic field vector, *b* = crystallographic *b* axis) is raised from *H* = 0 to *H* = 6 T, the intensity of the luminescence with polarization **E**∥*b* (**E** = electric field vector) increases by a factor of ~2. This result is explained by a magnetic field induced mixing of the two excited states of each trap. For **H**⊥*b* a strongly field-dependent nonradiative deactivation competes with the luminescence.

Introduction

Recently the optical properties of the cyclometalated homoleptic d^8 complexes [Pt(phpy)$_2$] (phpy = 2-phenylpyridinato) and [Pd(bhq)$_2$] (bhq = benzo[*h*]quinolinato) have been reported.[1,2]

Single-crystal [Pt(phpy)$_2$] exhibits an unstructured luminescence band. The energy and intensity of the luminescence depend on temperature and on the strength of an applied magnetic field, similar to the behavior that has been found for numerous cyanoplatinates(II),[3-8] binuclear platinum(II) complexes,[9] and tungsten pentacarbonyl crystals.[10] The experimental results could be explained by a model based on the existence of dimeric units (Pt–Pt distance 3.53 Å) in the solid state and the MLCT character

[†] Universität Regensburg.
[‡] University of Fribourg.

(1) Bär, L.; Gliemann, G.; Chassot, L.; von Zelewsky, A. *Chem. Phys. Lett.* **1986**, *123*, 264.
(2) Schwarz, R.; Gliemann, G.; Chassot, L.; von Zelewsky, A. *Inorg. Chem.*, in press.
(3) Hidvegi, I.; von Ammon, W.; Gliemann, G. *J. Chem. Phys.* **1982**, *76*, 4361.
(4) Hidvegi, I.; von Ammon, W.; Gliemann, G. *J. Chem. Phys.* **1984**, *80*, 2837.
(5) Dillinger, R.; Gliemann, G.; Pfleger, H. P.; Krogmann, K. *Inorg. Chem.* **1983**, *22*, 1366.
(6) Biedermann, J.; Wallfahrer, M.; Gliemann, G. *J. Lumin.* **1987**, *37*, 323.
(7) Schwarz, R.; Lindner, M.; Gliemann, G. *Ber. Bunsen-Ges. Phys. Chem.* **1987**, *91*, 1233.

0020-1669/89/1328-1053$01.50/0

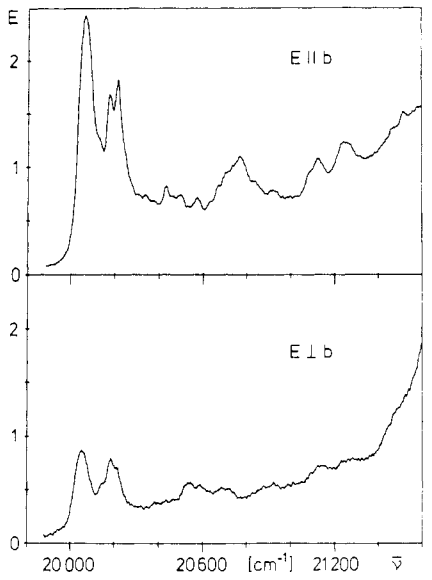

Figure 1. Polarized low-energy absorption spectra of single-crystal $[Pt(bhq)_2]$ (thickness ~20 μm) at T = 10 K.

of the low-energy absorption process in the solution.[12,13] In this model the luminescence is assigned to the radiative deactivation of two spin–orbit components of the energetically lowest triplet state.

In contrast to the case for $[Pt(phpy)_2]$ the polarized luminescence spectra of single-crystal $[Pd(bhq)_2]$ at T = 1.9 K exhibit a coarse structure superimposed by sharp lines in the high-energy range of the luminescence. With increasing temperature these sharp lines vanish and a fictitious red shift of the spectra results ($\Delta\bar{\nu}$ = 760 cm^{-1} at T = 60 K). Application of homogeneous magnetic fields ($H \leq 6$ T) does not influence the phosphorescence. In order to describe the experimental results, an energy level diagram has been developed, which is composed of the lowest triplet exciton band and distinct X-traps located energetically below this band. The single-crystal absorption and emission could be assigned to transitions within the ligand π electron system, which is disturbed by the central ion. This assignment agrees with that proposed by Balzani, von Zelewsky, et al.[12,13] for the corresponding solution spectra.

The purpose of this paper is to report on the polarized absorption and emission spectra of single-crystal $[Pt(bhq)_2]$ at different temperatures (1.9 K $\leq T \leq$ 60 K) and in homogeneous magnetic fields ($0 \leq H \leq 6$ T). The compound $[Pt(bhq)_2]$ promises to be an interesting tool for optical studies, because it occupies a position midway between the complexes $[Pd(bhq)_2]$ and $[Pt(phpy)_2]$ in the following sense. On the one hand, a stronger spin–orbit splitting of the lowest triplet states than for the palladium(II) compound is expected because of the larger spin–orbit constant of platinum(II). On the other hand, because of the larger Pt–Pt distance (4.30 Å[14]) than in the solid $[Pt(phpy)_2]$ and because of the spatial extent of the bhq ligands the formation of defect states due to impurities and lattice defects should be facilitated in single-crystal $[Pt(bhq)_2]$. For these reasons the low-temperature luminescence of single-crystal $[Pt(bhq)_2]$ should exhibit (i) a magnetic field dependence comparable to that of the compound

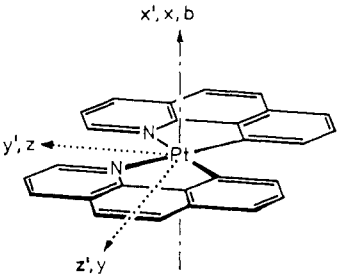

Figure 2. Schematic representation of the complex $[Pt(bhq)_2]$. x, y, and z denote the molecular axes of the complex, x', y', and z' denote the molecular axes of the free ligand bhq, and b denotes the crystallographic b axis.

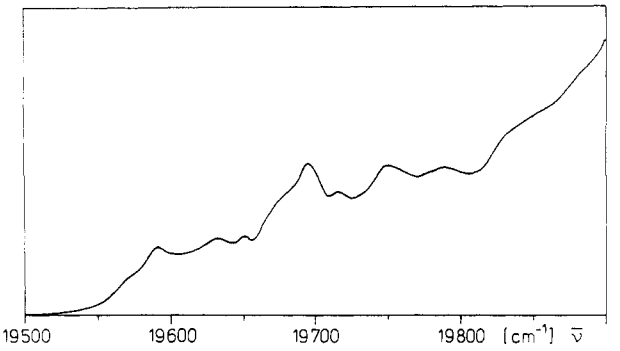

Figure 3. Excitation spectrum (nonpolarized) of single-crystal $[Pt(bhq)_2]$ at T = 7 K (λ_{det} = 526.3 nm).

$[Pt(phpy)_2]$ and (ii) highly structured spectra with sharp lines of X-trap emissions as observed for solid $[Pd(bhq)_2]$.

Experimental Section

$[Pt(bhq)_2]$ was prepared according to known methods.[11,15] For all measurements needle-shaped single crystals of size on the order of 5 × 0.1 × 0.05 mm^3 have been used.

All measurements were performed with a superconducting magnet system (Oxford Co., SM 4) yielding magnetic field strengths up to H = 6 T. As excitation sources for the cw emission spectra and the lifetime measurements an argon ion laser (λ_{exc} = 364 nm, Coherent Innovia 90) and a cavity dumped dye laser system (λ_{exc} = 435 nm, dye Cumarin 307), respectively, have been used.[16] The emitted light was selected by a double-grating monochromator (Spex 1404, Czerny–Turner mounting, 0.1-nm resolving power at 500 nm) and detected by an EMI S 20 multiplier. The polarization of the exciting laser beam was chosen parallel to the crystallographic b axis (parallel to the needle axis of the crystals), except the measurements with magnetic field orientation $\mathbf{H} \| b$, where the laser beam was polarized perpendicularly to the b axis. Further details of the instrumental device and the experimental methods concerning the polarized absorption and the excitation spectra are described elsewhere.[17,18]

Results

Figure 1 shows the polarized absorption spectra of single-crystal $[Pt(bhq)_2]$ at T = 10 K. The electric field vector $\mathbf{E}$ of the light has been chosen parallel and perpendicular to the crystallographic b axis, respectively (cf. Figure 2). A distinct dependence on polarization is observed for the half-widths, the intensities, and the energies of the absorption bands at the low-energy range of the spectra. The intense absorption bands with $\mathbf{E} \| b$ polarization (maximum at $\bar{\nu}_{\|}$ = 20050 cm^{-1}) and $\mathbf{E} \perp b$ polarization (maximum at $\bar{\nu}_{\perp}$ = 20038 cm^{-1}) are separated by $\Delta\bar{\nu}$ = 12 cm^{-1} and have half-widths of $\Delta\bar{\nu}_{\|}$ = 70 cm^{-1} and $\Delta\bar{\nu}_{\perp}$ = 110 cm^{-1}, respectively. With the molar concentration of $[Pt(bhq)_2]$ in the crystal, c = 3.68 mol·L^{-1},[14] the extinction coefficient of the intense $\mathbf{E} \| b$ absorption band can be estimated as $\epsilon_{\|} \approx$ 320 L·mol^{-1}·cm^{-1}. This value is higher by a factor of 200 than the corresponding ϵ value

(8) Gliemann, G.; Yersin, H. *Struct. Bonding* **1985**, *62*, 87.
(9) Bär, L.; Gliemann, G. *Chem. Phys. Lett.* **1984**, *108*, 14.
(10) Dillinger, R.; Gliemann, G. *Chem. Phys. Lett.* **1985**, *122*, 66.
(11) Chassot, L.; Müller, E.; von Zelewsky, A. *Inorg. Chem.* **1984**, *23*, 4249.
(12) Maestri, M.; Sandrini, D.; Balzani, V.; Chassot, L.; Jolliet, P.; von Zelewsky, A. *Chem. Phys. Lett.* **1985**, *122*, 375.
(13) Balzani, V.; Maestri, M.; Melandri, A.; Sandrini, D.; Chassot, L.; Cornioley-Deuschel, C.; Jolliet, P.; Maeder, U.; von Zelewsky, A. *Photochemistry and Photophysics of Coordination Compounds*; Yersin, H., Vogler, A., Eds.; Springer-Verlag: Berlin, Heidelberg, New York, 1987. Maestri, M.; Sandrini, D.; Balzani, V.; von Zelewsky, A.; Jolliet, P. *Helv. Chim. Acta* **1988**, *134*, 71.
(14) Bernardinelli, G.; Chassot, L.; von Zelewsky, A. Submitted for publication.
(15) Chassot, L.; von Zelewsky, A. *Inorg. Chem.* **1987**, *26*, 2814.
(16) von Ammon, W. Thesis, Regensburg, FRG, 1981.
(17) Tuszinsky, W.; Gliemann, G. *Ber. Bunsen-Ges. Phys. Chem.* **1985**, *89*, 940.
(18) Zimmermann, F. Thesis, Regensburg, FRG, 1986.

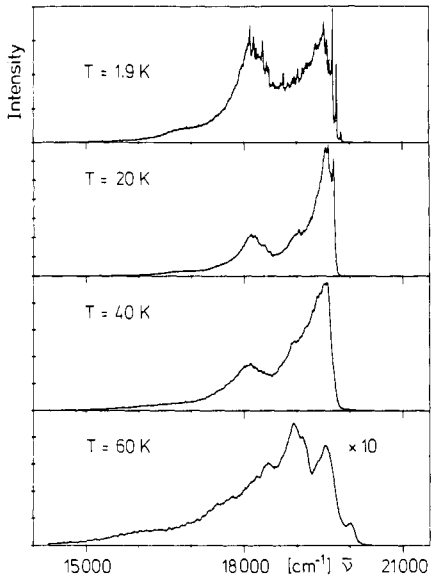

Figure 4. $\mathbf{E}\|b$ polarized emission spectra of single-crystal $[Pt(bhq)_2]$ at different temperatures ($\lambda_{exc} = 364$ nm).

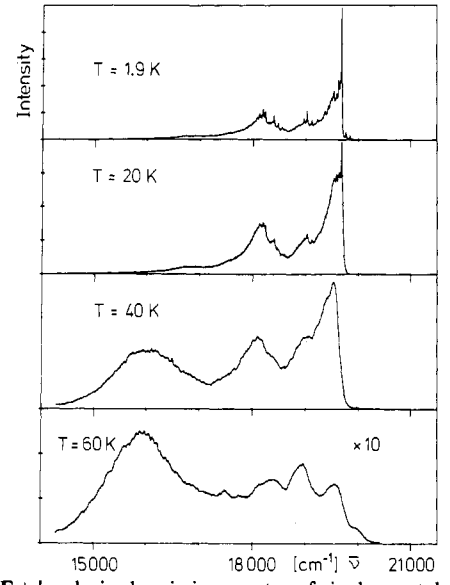

Figure 5. $\mathbf{E}\perp b$ polarized emission spectra of single-crystal $[Pt(bhq)_2]$ at different temperatures ($\lambda_{exc} = 364$ nm).

of the homologic Pd compound.[2] Raising the temperature from $T = 10$ K to room temperature does not influence the energies of the absorption bands, but the structure of the polarized spectra becomes more and more indistinct.

The nonpolarized excitation spectrum (detection wavenumber $\bar{\nu} = 19000$ cm^{-1}, $T = 7$ K) for the spectral range lower in energy than the absorption maxima is shown in Figure 3. This spectrum is not corrected for the wavelength dependence of the excitation intensity. Between $\bar{\nu} = 19500$ and 19900 cm^{-1} several excitation bands are resolved, indicating weak absorptions at $\bar{\nu} \approx 19550$ cm^{-1} and higher energies. The excitation spectrum has been found to be independent of the detection wavenumber.

The polarized emission spectra for 364-nm excitation at $T = 1.9$ K are presented in the upper parts of Figures 4 and 5. Both spectra are composed of several broad bands showing distinct fine structures. At the high-energy sections of these bands the fine-structure lines are relatively sharp and intense. In the $\mathbf{E}\|b$ polarized emission the intensities of the two broad bands of highest energy are comparable, whereas the $\mathbf{E}\perp b$ polarized emission is dominated by the one intense band of highest energy and the fine-structure line forming the top of this band. The expanded high-energy section of the polarized emission spectra is shown in Figure 6. Emission lines labeled by the same number in both

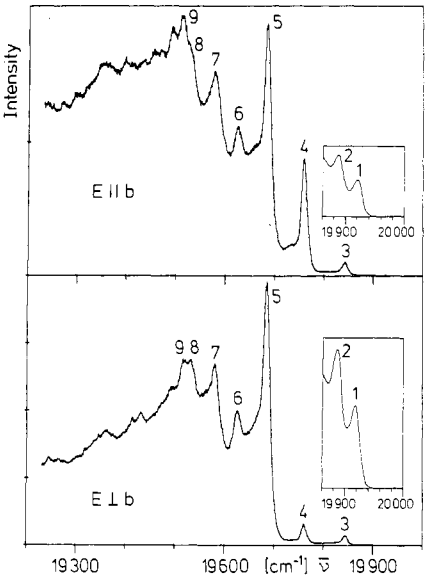

Figure 6. High-energy range of the polarized emission spectra of single-crystal $[Pt(bhq)_2]$ at $T = 1.9$ K ($\lambda_{exc} = 364$ nm).

polarized spectra have equal energy. The half-widths of the sharp peaks are found to be $\Delta\bar{\nu} \approx 20$ cm^{-1}. At the blue flank of the emission line labeled by number 3 there are two weak peaks (numbers 1 and 2), which are less intense by a factor of ~10 (cf. the inserts in Figure 6). The high-energy peaks differ in their intensity ratio $I_\parallel/I_\perp$ for both polarizations. Peak 4 is predominantly $\mathbf{E}\|b$ polarized; for the other lines the $\mathbf{E}\perp b$ component has the distinctly higher intensity. Because of these different polarization properties peaks 1, 3, 4, and 5 cannot be members of the same progression. A further important result is the energetic overlap of the emission spectra with the excitation spectrum by $\Delta\bar{\nu} \approx 400$ cm^{-1} (cf. Figures 3 and 6).

The influence of temperature on the polarized luminescence of single-crystal $[Pt(bhq)_2]$ is demonstrated in Figures 4 and 5. Note the different intensity scales! When the temperature is raised from $T = 1.9$ to 20 K, the sharp lines of the high-energy section vanish successively one by one and simultaneously for both polarizations, an effect that has been observed also for the homologeous Pd complex.[2] The fine structure of the low-energy section does not change considerably between $T = 1.9$ and 20 K for $\mathbf{E}\perp b$ polarization. For $\mathbf{E}\|b$ polarization, however, the low-energy fine structure vanishes already at $T = 5$ K, together with peaks 1 and 2. Further increase of temperature to $T = 40$ K distinctly reduces the fine structure for both polarizations, and only coarsely structured emission spectra without any sharp lines result. In the $\mathbf{E}\perp b$ polarized spectrum an additional broad band with a maximum at $\bar{\nu} \approx 16000$ cm^{-1} is observed. This band dominates the $\mathbf{E}\perp b$ spectrum if the temperature is increased to $T = 60$ K. Between $T = 40$ and 60 K at the high-energy side of the emission spectra further additional bands grow out, changing completely the coarse structure of the spectra. Within the experimental error the energy of the blue bands ($\bar{\nu} \approx 20030$ cm^{-1}) coincides with the energies of the absorption bands ($\mathbf{E}\perp b$, $\bar{\nu} = 20038$ cm^{-1}; $\mathbf{E}\|b$, $\bar{\nu} = 20050$ cm^{-1}).

The temperature dependence of the emission intensity can be divided into two stages. Between $T = 1.9$ and 30 K the $\mathbf{E}\perp b$ intensity is constant; the $\mathbf{E}\|b$ intensity, however, is increased by a factor of ~1.4. Temperature increase from $T = 30$ to 60 K reduces the quantum yield of both polarized emissions by factors of ~0.2 ($\mathbf{E}\perp b$) and ~0.3 ($\mathbf{E}\|b$), respectively.

Details of the temperature dependence of the $\mathbf{E}\|b$ emission are given in Figure 7, which shows the expanded high-energy section of the $\mathbf{E}\|b$ spectrum at $T = 1.9$, 5, 10, and 15 K. The intensities are normalized to unity with respect to the most intense peak. With increasing temperature the maximum of peak 4 is blue-shifted. All other sharp peaks in the high-energy range lose intensity, and at the blue flank of each peak a new line grows out finally surpassing the intensity of the initial peak. The energy

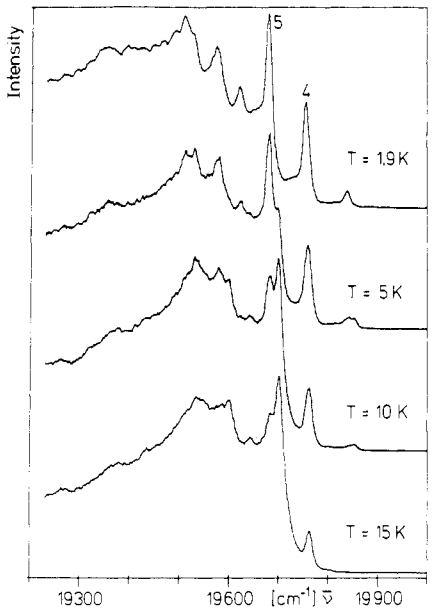

Figure 7. High-energy range of the $\mathbf{E}\|b$ polarized emission spectra of single-crystal $[Pt(bhq)_2]$ at low temperatures (1.9 K $\leq T \leq$ 15 K; λ_{exc} = 364 nm).

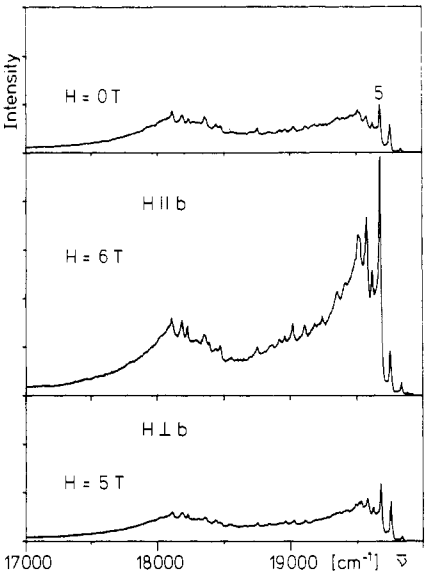

Figure 8. $\mathbf{E}\|b$ polarized emission spectra of single-crystal $[Pt(bhq)_2]$ at H = 0 and at magnetic fields $\mathbf{H}\|b$ (H = 6 T) and $\mathbf{H}\perp b$ (H = 5 T) (λ_{exc} = 364 nm, T = 1.9 K).

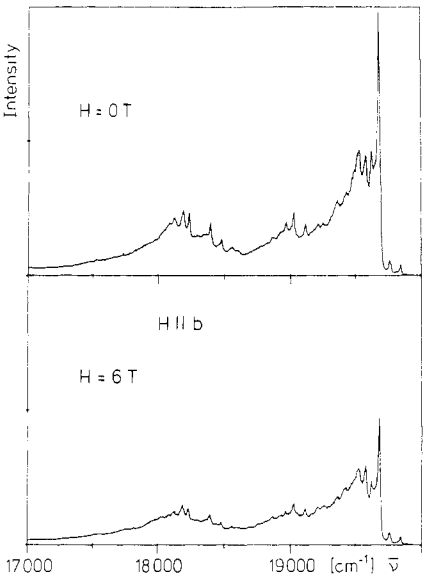

Figure 9. $\mathbf{E}\perp b$ polarized emission spectra of single-crystal $[Pt(bhq)_2]$ at H = 0 and H = 6 T (orientation of the magnetic field $\mathbf{H}\|b$, λ_{exc} = 364 nm, T = 1.9 K).

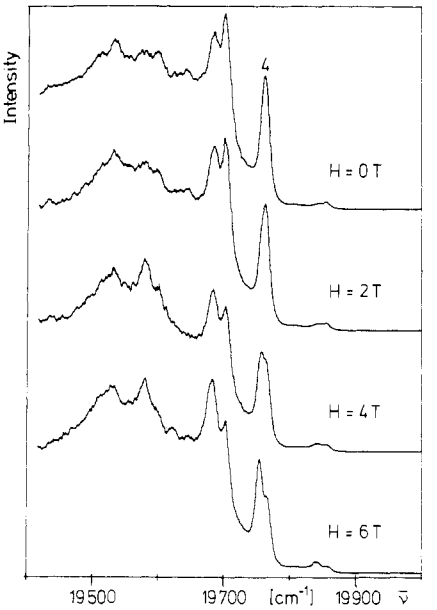

Figure 10. High-energy range of the $\mathbf{E}\|b$ polarized emission spectra of single-crystal $[Pt(bhq)_2]$ at different magnetic field strengths (orientation of the magnetic field $\mathbf{H}\perp b$, λ_{exc} = 364 nm, T = 10 K).

separation between the maxima of the pair of peaks with label 5 is estimated to be $\Delta\bar{\nu}$ = 20 cm^{-1}.

The decay of the luminescence at T = 1.9 K is monoexponential with a lifetime of $\tau \approx 26$ μs and independent of the polarization and the wavelength of the emission, except peak 4, which shows a nonexponential decay. At higher temperatures all peaks with temperature-dependent intensity display a distinct nonexponential decay, and thus, no intrinsic lifetime could be specified. A similar behavior has been found for single-crystal $[Pd(bhq)_2]$.[2] The broad $\mathbf{E}\perp b$ polarized emission band (at $\bar{\nu} \approx 16\,000$ cm^{-1}, cf. Figure 5) exhibits initially a plain rise of luminescence.

Application of a homogeneous magnetic field $\mathbf{H}\|b$ at T = 1.9 K influences strongly the polarized emission of single-crystal $[Pt(bhq)_2]$ (cf. Figures 8 and 9). Raising the magnetic field strength from H = 0 to 6 T doubles the integral intensity of the $\mathbf{E}\|b$ emission, mainly due to an increase of the high-energy part of the emission. As Figure 8 illustrates, the intensity ratio $I(H = 6\text{ T})/I(H = 0)$ varies for the different high-energy peaks. For peak 5 a ratio of ~5.5 was found. The magnetic field induced intensity increase is always a purely quadratic function of H. Between H = 0 and 6 T the intensity of the $\mathbf{E}\perp b$ emission is reduced by a factor of ~1.3 (cf. Figure 9). It is amazing that the $\mathbf{E}\|b$ spectrum at field strength H = 6 T with $\mathbf{H}\|b$ agrees largely with the zero-field $\mathbf{E}\perp b$ spectrum. At H = 6 T the high-energy peaks show a Zeeman red shift of $\Delta\bar{\nu} \approx 4$ cm^{-1}, independent of the polarization.

Homogeneous magnetic fields of orientation $\mathbf{H}\perp b$ change the $\mathbf{E}\|b$ emission at T = 1.9 K in a completely different way. By the magnetic field the sharp peaks at the high-energy side of the emission spectrum are only slightly increased; the low-energy part of the emission, however, is even drastically reduced, as Figure 8 shows. Thereby, the quantum yield of the total $\mathbf{E}\|b$ emission is lowered by 25%, when the magnetic field strength is raised from H = 0 to 5 T. The intensity and the quantum yield of the $\mathbf{E}\perp b$ emission are independent of the magnetic field $\mathbf{H}\perp b$. The high-energy peaks of both the $\mathbf{E}\|b$ and the $\mathbf{E}\perp b$ emission exhibit a Zeeman red shift of several wavenumbers at H = 6 T.

In order to demonstrate the magnetic field effects on the emission at higher temperatures, Figure 10 presents the high-energy range of the $\mathbf{E}\|b$ emission at T = 10 K and at different

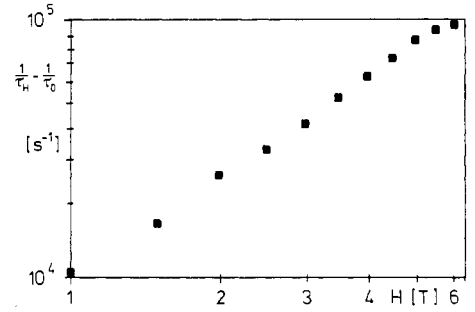

Figure 11. Magnetic field dependence of the deactivation rate of the $\mathbf{E}\|b$ polarized emission of single-crystal [Pt(bhq)$_2$] (orientation of the magnetic field $\mathbf{H}\perp b$, λ_{exc} = 364 nm, λ_{det} = 508.1 nm, T = 1.9 K).

field strengths with $\mathbf{H}\perp b$. A comparison of the line patterns of the spectra at $H = 0$ and $H > 0$, respectively, shows an important regularity for each pair of peaks. That peak which has been induced by temperature increase vanishes with increasing magnetic field strength, whereas the low-temperature peak simultaneously gains intensity. Even at the high-energy flank of peak 4 a shoulder appears, indicating an intensity exchange between energetically nearby peaks ($\Delta\bar{\nu} < 20$ cm^{-1}). Magnetic fields of $\mathbf{H}\|b$ orientation cause qualitatively similar, but even more intense, effects.

In contrast to the shapes of the emission spectra the emission decay rates react only on perturbations by magnetic fields of orientation $\mathbf{H}\perp b$. At T = 1.9 K the decay curves are monoexponential at all field strengths. The slopes of the decay curves, however, vary with the emission wavelength but not with the polarization of the emission. For example, raising the field strength from $H = 0$ to 6 T shortens the lifetime of peak 5 (cf. Figure 6) from τ = 26 to 7.5 μs. Figure 11 shows a log–log plot of the corresponding deactivation rate $1/\tau(H) - 1/\tau(H = 0)$ versus the magnetic field strength H. Within the limits of experimental error a graph with slope $\sim$1.3 results.

Discussion

The structure of the approximately planar complex [Pt(bhq)$_2$] is given schematically in Figure 2. The molecular x axis is perpendicular to the plane of the complex and coincides with the crystallographic b axis.[14] The 2-fold symmetry axis bisecting the C–Pt–C angle defines the molecular z axis. The symmetry of the Pt ion with its first coordination sphere can be described approximately by the point group C_{2v} (double group C_{2v}'); the real site symmetry, however, is a lower one.[14] As shown by indexing of the crystal faces, the needle axis of the crystal is parallel to the crystallographic b axis.[14,19]

Due to the electronic similarities of the ligands bhq and o-phen (*o*-phenanthroline, symmetry C_{2v}) the symmetries of the HOMO and the LUMO of the free ligand bhq can be assigned to the irreducible representations b_1 and a_2 of the point group C_{2v}, respectively.[20] Considering the different orientations of the principal axes of the free ligand and the complex (cf. Figure 2), the HOMO and the LUMO of the pair $(bhq)_2$ of the complex transform as a_2 and b_1, respectively.

In a ligand field of symmetry C_{2v} the five metal d states split according to the energetic order[6,7,21]

$$1a_1(x^2) < 1b_1(xz),\ 1a_2(xy) < 2a_1(y^2 - z^2) \ll 1b_2(yz)$$

The state $1b_2(yz)$ is expected to be shifted energetically above the metal 6s state by a strong ligand field.[6,7,21] Since the low-energy absorption in solution spectra of ortho-metalated Pt(II) complexes could be assigned to MLCT transitions,[11-13] the LUMO b_1 of the pair $(bhq)_2$ must be the LUMO of the single complex, and a metal d state constitutes the HOMO of the complex. For symmetry reasons an admixture of the HOMO a_2 of the pair $(bhq)_2$ to the metal d state $1a_2(xy)$ is expected, shifting $1a_2(xy)$ energetically above the metal d state $2a_1(y^2 - z^2)$. Therefore, the HOMO of the single complex gets partially ligand character and transforms according to a_2.

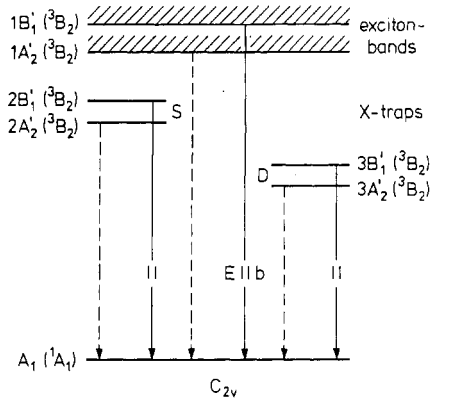

Figure 12. Proposed energy level diagram of single-crystal [Pt(bhq)$_2$] (S, shallow X-trap; D, deep X-trap).

In the case of $C_{2v}'(C_{2v})$ symmetry the ground-state configuration of a single complex yields the term $A_1'(^1A_1)$. From the energetically lowest excited configuration the terms $A_1', A_2', B_1'(^3B_2)$ and $B_2'(^1B_2)$ result. As will be shown below from the experimental results, the spin–orbit components of $^3B_2$ parentage are the lowest excited states and have the following energetic order: $A_2' < B_1' < A_1'$. A group-theoretical analysis predicts electric-dipole-allowed transitions between the ground state A_1' and the excited states A_1' and B_1' with $\mathbf{E}\perp b$ and $\mathbf{E}\|b$ polarization, respectively. The transition between the ground state and the excited state A_2' is forbidden.

In the solid state the excited states form energy bands. For the interpretation of the optical properties of single-crystal [Pt(bhq)$_2$] an energy level diagram will be applied, originally developed to describe optical properties of crystalline organic compounds[22-27] and recently approved to explain the solid-state emission of [Pd(bhq)$_2$].[2] As excited states this model considers one exciton band and X-traps with one respective sharp energy level below the exciton band. The X-traps are assumed to be due to [Pd(bhq)$_2$] complexes that are disturbed by impurities or defects in the crystal.

In order to explain our experimental results for single-crystal [Pt(bhq)$_2$], the energy level diagram developed in ref 2 for [Pd(bhq)$_2$] has to be modified. For [Pt(bhq)$_2$] two exciton bands and two excited states per X-trap are required, as shown in Figure 12. To simplify matters, only two traps, a shallow trap S and a deep trap D with stabilization energies ΔE_S and ΔE_D, respectively, are considered. The arrows indicate the electric-dipole-allowed (solid arrow) and -forbidden (dashed arrow) transitions.

The strong $\mathbf{E}\|b$ polarized absorption band (cf. Figure 1) can be assigned to the transition from the ground electronic state $A_1'(^1A_1)$ to the exciton band $B_1'(^3B_2)$. According to the MLCT character of the transition and the relatively large spin–orbit coupling constant of the Pt ion the extinction coefficient is higher than that of the homologic Pd compound.[2] The less intense $\mathbf{E}\perp b$ polarized absorption band corresponds to the excitation to the exciton band $A_2'(^3B_2)$. This transition, which is electric-dipole-forbidden in C_{2v} symmetry, gains intensity by an admixture of other states due to the lower site symmetry and/or by vibronic coupling. The latter mechanism causes the relatively large half-width of the $\mathbf{E}\perp b$ absorption band. It cannot be ruled out that the transition $A_1'(^1A_1) \rightarrow A_2'(^3B_2)$ is present in the $\mathbf{E}\|b$ spectrum, but in this case it is obscured by the more intense

(19) Schwarz, R.; Gliemann, G. Unpublished results.
(20) Heilbronner-Straub. *Hückel-Molecular Orbitals*; Springer-Verlag: Berlin, Heidelberg, New York, 1966.
(21) Isci, H.; Mason, W. R. *Inorg. Chem.* **1975**, *14*, 905.
(22) Güttler, W.; von Schütz, J. U.; Wolf, H. C. *Chem. Phys.* **1977**, *24*, 159.
(23) Weinzierl, G.; Friedrich, J. *Chem. Phys. Lett.* **1981**, *83*, 204.
(24) Komada, Y.; Yamauchi, S.; Hirota, N. *J. Chem. Phys.* **1985**, *82*, 1651.
(25) Vala, M.; Baiardo, J.; Wierzbicki, A.; Trabjerg, J. *Chem. Phys.* **1987**, *116*, 221.
(26) Fayer, M. D.; Harris, C. B. *Phys. Rev. B* **1974**, *9*, 748.
(27) Shelby, R. M.; Zewail, A. H.; Harris, C. B. *J. Chem. Phys.* **1976**, *64*, 3192.

absorption $A_1'(^1A_1) \rightarrow B_1'(^3B_2)$. The weak low-energy bands in the excitation spectrum correspond to absorption by different types of X-traps.

Depending on the temperature, the emission processes start either from X-trap states or from exciton bands. After the excitation of the crystal the exciton bands are populated by a nonradiative relaxation. The excitation energy migrates within the exciton bands, and finally it will be localized at a X-trap. At $T = 1.9$ K the trapping process ends in $A_2'(^3B_2)$, the energetically lowest excited state of the respective trap. Energy transfer between the traps via the exciton bands can be neglected at $T = 1.9$ K, and thus, the emission is a superposition of the luminescence of all types of X-traps. The intense and sharp emission peaks in the high-energy range of the polarized spectra (cf. Figures 4 and 5) are assigned to 0–0 transitions of different types of X-traps. Since for C_{2v}' symmetry these transitions are electric-dipole-forbidden, their occurrence in the spectra indicates that the site symmetry of the traps is lower than C_{2v} as expected from the crystallographic data.

When the temperature is raised from $T = 1.9$ to ~ 20 K, traps will be depleted and a thermal repopulation of the exciton bands occurs. Corresponding to the individual temperature dependence of the detrapping rates and to the stabilization energies of the different X-trap types, the respective 0–0 transitions and their vibronic satellites vanish one by one with increasing temperature, beginning with the peaks of highest energy (cf. Figures 4 and 5). Since the vibronic structure in the $\mathbf{E}\|b$ spectrum disappears already at $T \approx 5$ K, together with peaks 1 and 2, this vibronic structure can be assigned to vibronic transitions of X-traps of type 1 or 2, respectively. At $\mathbf{E}\|b$ polarization another mechanism is competing with the detrapping process. The trap states $B_1'(^3B_2)$ higher in energy by $\Delta\bar{\nu} \approx 20$ cm^{-1} than the states $A_2'(^3B_2)$ become thermally repopulated, and thus, the allowed radiative deactivations $B_1' \rightarrow A_1'$ with $\mathbf{E}\|b$ polarization become effective (cf. Figure 12). This explains why with increasing temperature at the blue flanks of the low-temperature peaks additional lines grow out (cf. Figure 7) together with an increase of the $\mathbf{E}\|b$ quantum yield. Such an additional line is missing for peak 4. This result can be understood, if the energy gap between the excited states $A_2'(^3B_2)$ and $B_1'(^3B_2)$ of the corresponding X-trap is much smaller than 20 cm^{-1}. For such a small energetical separation thermal repopulation is efficient already at $T = 1.9$ K. That explains also the special polarization ratio (cf. Figure 6) and the decay behavior of peak 4.

Further temperature increase to $T = 60$ K establishes thermal equilibrium between the exciton bands and the excited states of all traps. In contrast to the case for single-crystal $[Pd(bhq)_2]$ very deep traps ($E_D \geq 800$ cm^{-1}) that cannot be thermally depleted at $T = 60$ K have not been observed in the platinum system. The occupied exciton bands $B_1'(^3B_2)$ and $A_2'(^3B_2)$ are deactivated radiatively, yielding the broad emission bands at $\bar{\nu} \approx 20030$ cm^{-1} with $\mathbf{E}\|b$ and $\mathbf{E}\perp b$ polarization, respectively (cf. Figures 4 and 5). The small energy separation between these high-energy emission bands and the intense absorption bands corroborates the proposed assignments. Unfortunately it could not be decided whether the broad $\mathbf{E}\perp b$ emission at $\bar{\nu} \approx 16000$ cm^{-1} belongs to the emission of an impurity or to an unstructured X-trap luminescence.[24] The reduction of the integral quantum yield between $T = 30$ and 60 K probably results from a nonradiative deactivation with a temperature-dependent rate.

According to the relatively strong spin–orbit coupling in Pt(II) and to the LMCT character of the luminescence the emission lifetime $\tau = 26$ μs of $[Pt(bhq)_2]$ is shortened compared to the value $\tau = 85$ μs of $[Pd(bhq)_2]$. The reduction of the emission lifetime at higher temperatures can be traced back to the increasing thermal repopulation of the states of $B_1'(^3B_2)$. The simultaneous loss of the monoexponential character of the decay is probably due to the competitive processes of trapping and detrapping. The rise rate of the broad $\mathbf{E}\perp b$ emission band at $\bar{\nu} \approx 16000$ cm^{-1} can be explained by an energy transfer.

Application of a homogeneous magnetic field lowers the symmetry of the complex. The left-hand side of Figure 13 shows the energy level diagram of $[Pt(bhq)_2]$ in a magnetic field $\mathbf{H}\|b$ ($\mathbf{H}\|x$)

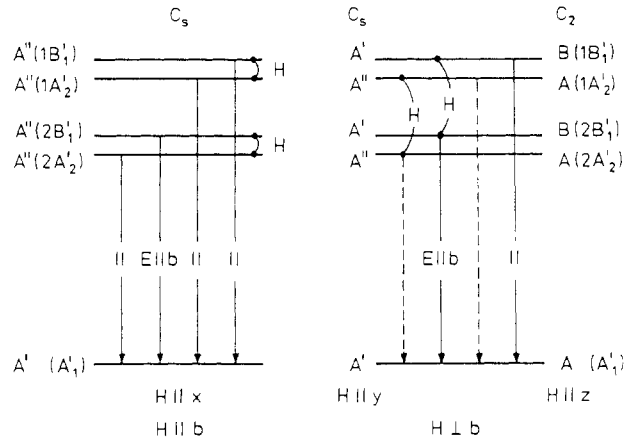

Figure 13. Proposed energy level diagrams of single-crystal $[Pt(bhq)_2]$ at applied homogeneous magnetic fields: (left) $\mathbf{H}\|b$; (right) $\mathbf{H}\perp b$.

and the selection rules for electric dipole transitions. The perturbed complex has the point symmetry C_s. For this symmetry both spin–orbit components $A_2'(^3B_2)$ and $B_1'(^3B_2)$ of a trap transform according to the same irreducible representation A'' of C_s symmetry and can mix. Thus, the transition from the states $A_2'(^3B_2)$ to the ground state $A_1'(^1A_1)$ becomes electric-dipole-allowed with $\mathbf{E}\|b$ polarization. Since the degree of admixture of the wave functions is in a first approximation proportional to the reciprocal value of the energy gap between the mixing states, the magnetic field induced intensity increase will be different for each X-trap type. Additionally a Zeeman repulsion of the mixing states is expected. Both effects mentioned above have been observed, the Zeeman red shift of the 0–0 transitions and the intensity increase of the $\mathbf{E}\|b$ polarized luminescence at $T = 1.9$ K, as shown by Figure 8. The experimental result $I_\| \approx H^2$, with $I_\|$ being the intensity of the $\mathbf{E}\|b$ polarized peaks, is in complete agreement with predictions of quantum-mechanical perturbation theory.[8,28,29] The observed intensity decrease of the $\mathbf{E}\perp b$ luminescence is not induced by a lowering of the transition probability for this polarization but by the higher deactivation rate of the $\mathbf{E}\|b$ component.

At $T \geq 10$ K and $H = 0$ the $\mathbf{E}\|b$ emission is dominated by the transitions $B_1'(^3B_2) \rightarrow A_1'(^1A_1)$. When the magnetic field $\mathbf{H}\|b$ is switched on, the allowed transitions $A''(A_2') \rightarrow A'(A_1')$ compete with the transitions $A''(B_1') \rightarrow A'(A_1')$ and, in addition, the Boltzmann distribution for the states $A''(A_2')$ and $A''(B_1')$ is changed as a result of the Zeeman repulsion. Thus, with increasing field strength the emission from the states $A''(A_2')$ gains intensity. That explains why for each pair of emission peaks the intensity of the low-energy peak increases with a magnetic field and at high field strengths even surpasses the intensity of the temperature-induced high-energy peak. The formation of the narrow double structure of peak 4 at $H \gtrsim 3$ T (cf. Figure 10) verifies the above assumption that the states $A_2'(^3B_2)$ and $B_1'(^3B_2)$ of the corresponding trap have a very small energy distance ($\Delta\bar{\nu} \ll 20$ cm^{-1}).

By a magnetic field $\mathbf{H}\perp b$ the symmetry of the complex is lowered to C_2 for $\mathbf{H}\|z$ and to C_s for $\mathbf{H}\|y$ as shown at the right-hand side of Figure 13. A mixing of states $A_2'(^3B_2)$ and $B_1'(^3B_2)$ is symmetry forbidden, and therefore, an additional radiative transition $A_2'(^3B_2) \rightarrow A_1'(^1A_1)$ is not allowed in contrast to the case $\mathbf{H}\|b$. Since the $\mathbf{E}\|b$ polarized emission decreases with increasing magnetic field strength at $T = 1.9$ K (cf. Figure 8), it seems probable that the nonradiative deactivation rate of the trap states $A_2'(^3B_2)$ is considerable already at $H = 0$ and is further increased by a magnetic field. Quantum-mechanical perturbation theory predicts for this case the following magnetic field dependence of the deactivation rate of the emission: $1/\tau(H) - 1/\tau(H = 0) = aH + bH^2$ (a and b are constants).[29] The experimental

(28) Gliemann, G. *Comments Inorg. Chem.* **1986**, *5*, 263.
(29) Gliemann, G. *31st International Congress of Pure and Applied Chemistry* [*Proceedings*]; Sofia, Bulgaria; Pergamon: Oxford, England, 1987; Inorganic Chemistry p 11.

results are compatible with this prediction. For $\mathbf{H} \perp b$ as well the observed slight intensity increase and the red shift of the high-energy peaks at $T = 1.9$ K, as the other magnetic field effects at $T \geq 10$ K (cf. Figure 10), may be caused by a small misalignment of the applied magnetic field, yielding an admixture of $\mathbf{H} \parallel b$ with the supposed $\mathbf{H} \perp b$ field.

Acknowledgment. This research has been supported by the Deutsche Forschungsgemeinschaft, the Fonds der Chemischen Industrie, and the Swiss National Science Foundation.

Contribution from the Department of Chemistry and Illinois ESR Research Center, University of Illinois at Urbana-Champaign, 505 South Mathews Avenue, Urbana, Illinois 61801

EPR-Derived Electronic Characteristics of Zerovalent Manganese Carbonyl Di(tertiary phosphine) Radicals

Gail B. Rattinger, R. Linn Belford,* Howard Walker, and T. L. Brown*

Received November 4, 1987

Persistent $Mn(CO)_3L_2$ metal-centered radicals, where the ligand, L, is either a tertiary phosphine or phosphite, are isoelectronic with the pentacyanocobaltate radical anion, $Co(CN)_5^{3-}$, a well-characterized radical,[6] and with the unsubstituted manganese(0) pentacarbonyl radical. This paper presents a characterization via multifrequency EPR spectroscopy of a series of $\cdot Mn(CO)_3L_2$ radicals—$\cdot Mn(CO)_3[P(n\text{-}Bu)_3]_2$, $\cdot Mn(CO)_3[P(i\text{-}Bu)_3]_2$, $\cdot Mn(CO)_3[P(i\text{-}Pr)_3]_2$, and $\cdot Mn(CO)_3[P(O\text{-}i\text{-}Pr)_3]_2$. Anisotropic g shifts and metal hyperfine and phosphorus superhyperfine spin Hamiltonian parameters are reported and compared to values reported in the literature for $\cdot Mn(CO)_5$. It is thus possible to examine some of the effects of varying ligand, geometry, and electronic parameters upon the characteristics of the EPR spectra obtained and upon the unpaired spin density localized in the manganese $3d_{z^2}$ and 4s metal orbitals and delocalized onto the phosphorus ligands. An LCAO–MO perturbation treatment of g and A values for these square-pyramidal d^7 systems yields reasonable estimates of the distribution of unpaired spin density, upper and lower limits of core polarization, and the energy difference, ΔE, between the ground state and $d\pi$ excited state.

Introduction

Interest in organometallic species has grown steadily over the last 40 years. Seventeen-electron (17e) organometallic free radicals and their reaction pathways have been of particular interest on account of their possible roles in homogeneous catalysis.[1-7] There have been numerous studies of the participation of metal-centered organometallic species in hydride abstraction,[8-10] electron transfers,[11-13] ligand substitutions,[4,8,13b,14-16] atom transfers,[3,9,17] and oxidative additions/reductive eliminations.[3,18] Because of rapid radical recombination it is difficult to prepare persistent zerovalent manganese-centered radicals; consequently, few examples are found in the literature.[9,10] Persistent $Mn(CO)_3L_2$ metal-centered radicals have been generated, where the ligand, L, is either a tertiary phosphine or phosphite.[9,10,19] These species are isoelectronic with the pentacyanocobaltate radical anion, $Co(CN)_5^{3-}$, a well-characterized radical,[6] and with the unsubstituted manganese(0) pentacarbonyl radical.[21,22] This paper presents a characterization via multifrequency EPR spectroscopy of a series of $\cdot Mn(CO)_3L_2$ radicals. We chose to study $\cdot Mn(CO)_3[P(n\text{-}Bu)_3]_2$, $\cdot Mn(CO)_3[P(i\text{-}Bu)_3]_2$, $\cdot Mn(CO)_3[P(i\text{-}Pr)_3]_2$, and $\cdot Mn(CO)_3[P(O\text{-}i\text{-}Pr)_3]_2$ in order to examine the effects of varying steric and electronic parameters[23,24] upon the characteristics of the EPR spectra obtained and upon the unpaired spin density localized in the manganese $3d_{z^2}$ and 4s metal orbitals and delocalized onto the phosphorus ligands. Anisotropic g shifts and metal hyperfine and phosphorus superhyperfine spin Hamiltonian parameters are reported and compared to values reported for $\cdot Mn(CO)_5$.[21] An LCAO–MO perturbation treatment of g and A values for these square-pyramidal d^7 systems yields reasonable estimates of the distribution of unpaired spin density, upper and lower limits of core polarization, and the energy difference, ΔE, between the ground state and $d\pi$ excited state. A less detailed study of $\cdot Mn(CO)_3L_2$ radicals has previously appeared.[25]

Experimental Section

All of the manganese radical samples were synthesized according to reported procedures.[9,10,19] The samples were transferred on a vacuum line directly into quartz EPR tubes, which were sealed for detachment to protect the air-sensitive radical. All of the samples were within a concentration range of 0.54–1.0 mM in hexane. The samples were then quickly frozen by immersion in liquid nitrogen and stored at 77 K. Useful lifetimes of samples kept in this way ranged from a few weeks to a maximum of 3 months. The quick freezing promoted good glassing,

(1) Brown, T. L. *Ann. N.Y. Acad. Sci.* **1980**, *330*, 80.
(2) Kochi, J. K. *J. Organomet. Chem.* **1986**, *300*, 139.
(3) (a) Wegman, R. W.; Brown, T. L. *Organometallics* **1982**, *1*, 47. (b) McCullen, S. B.; Brown, T. L. *Inorg. Chem.* **1981**, *20*, 3528.
(4) Forbus, N. P.; Brown, T. L. *Inorg. Chem.* **1981**, *20*, 4343.
(5) Kwiatek, J. *Catal. Rev.* **1967**, *1*, 37.
(6) Chock, P. B.; Dewar, R. B. K.; Halpern, J.; Wong, L. *J. Am. Chem. Soc.* **1969**, *91*, 82. Chock, P. B.; Halpern, J. *J. Am. Chem. Soc.* **1969**, *91*, 582.
(7) Lappert, M. F.; Lednor, P. W. *Adv. Organomet. Chem.* **1976**, *14*, 345.
(8) Byers, B. H.; Brown, T. L. *J. Am. Chem. Soc.* **1977**, *99*, 2527.
(9) McCullen, S. B.; Brown, T. L. *J. Am. Chem. Soc.* **1982**, *104*, 7496.
(10) Kidd, D. R.; Cheng, C. P.; Brown, T. L. *J. Am. Chem. Soc.* **1978**, *100*, 4103.
(11) (a) Kochi, J. K. *Acc. Chem. Res.* **1974**, *7*, 351. (b) Kochi, J. K. *Organometallic Mechanisms and Catalysis*; Academic: New York, 1978.
(12) Marzilli, L. G.; Marzilli, P. A.; Halpern, J. *J. Am. Chem. Soc.* **1970**, *92*, 5752.
(13) (a) Hepp, A. F.; Wrighton, M. S. *J. Am. Chem. Soc.* **1981**, *103*, 1258. (b) Meyer, T. J.; Caspar, J. V. *Chem. Rev.* **1985**, *85*, 187.
(14) Nubel, P. O.; Brown, T. L. *J. Am. Chem. Soc.* **1982**, *104*, 4955.
(15) Hoffman, N. W.; Brown, T. L. *Inorg. Chem.* **1978**, *17*, 613.
(16) Darensbourg, D. J. *Adv. Organomet. Chem.* **1982**, *21*, 113.
(17) Hanckel, J. M.; Lee, K.-W.; Rushman, P. R.; Brown, T. L. *Inorg. Chem.* **1986**, *25*, 1852.
(18) Halpern, J. *Acc. Chem. Res.* **1970**, *3*, 386.
(19) Kidd, D. R.; Brown, T. L. *J. Am. Chem. Soc.* **1978**, *100*, 4095.
(20) Herberhold, M.; Razavi, A. *Angew. Chem., Int. Ed. Engl.* **1975**, *14*, 351.
(21) Howard, J. A.; Morton, J. R.; Preston, K. F. *Chem. Phys. Lett.* **1981**, *83*, 226.
(22) Symons, M. C. R.; Sweany, R. L. *Organometallics* **1982**, *1*, 834.
(23) (a) Tolman, C. A. *J. Am. Chem. Soc.* **1970**, *92*, 2953. (b) Tolman, C. A. *J. Am. Chem. Soc.* **1970**, *92*, 2956.
(24) Tolman, C. A. *Chem. Rev.* **1977**, *77*, 313.
(25) Cheng, A. H.; Shyong, P. J. *Proc. Natl. Sci. Counc., Repub. China, Part B* **1982**, *6*, 298.

0020-1669/89/1328-1059$01.50/0